Giant resonances in ^{46,48}Ti

Y. Tokimoto, Y.-W. Lui, H. L. Clark, B. John,* X. Chen, and D. H. Youngblood
Cyclotron Institute, Texas A&M University, College Station, Texas 77843, USA
(Received 30 June 2006; published 24 October 2006)

The giant resonance region from 9 MeV $< E_x <$ 55 MeV in ^{46}Ti and ^{48}Ti has been studied with inelastic scattering of 240 MeV α particles at small angles including 0°. Isoscalar monopole strength in ^{46}Ti (^{48}Ti) was found corresponding to have 71 + 15/−12% (96 + 14/−12%) of the $E0$ energy weighted sum rule (EWSR) with a centroid of 18.66 + 0.65/−0.25 MeV (18.80 + 0.45/−0.18 MeV), respectively. In ^{46}Ti (^{48}Ti), 46±12% (56±12%) of the $E1$, and 60±11% (87±11%) of the $E2$ EWSR were identified.

DOI: 10.1103/PhysRevC.74.044308 PACS number(s): 25.55.Ci, 24.30.Cz, 27.40.+z

I. INTRODUCTION

The giant resonances are small amplitude collective modes of excitations of nuclei and have been extensively studied for several decades over a wide mass region [1,2]. The study of the isoscalar giant monopole resonance (ISGMR), in which protons and neutrons in a nucleus move in-phase and oscillate with spherical symmetry, is important because its energy (E_{GMR}) is related to the incompressibility of nuclear matter (K_{nm}) [3,4]. In the scaling model, the energy of GMR is given by $E_{\mathrm{GMR}} = (m_3/m_1)^{1/2}$, where $m_k = \sum(E_n - E_0)^k| < 0|r^2|n > |^2$. Most of the isoscalar $E0$ strength has been reported for ^{40}Ca (E_{GMR} of 20.42 + 0.89/−0.36 MeV) [5] and ^{58}Ni (E_{GMR} of 20.81 + 0.90/−0.28 MeV) [6] using inelastic α scattering. The GMR energy in ^{40}Ca is in agreement with the calculation by Nayak *et al.* [7] using the SkM* interaction, whereas that in ^{58}Ni is about 1 MeV higher than the calculation. Consequently we have studied the giant resonances in ^{46,48}Ti which lie between ^{40}Ca and ^{58}Ni in the mass region.

II. EXPERIMENTAL TECHNIQUE AND DATA ANALYSIS

The experimental technique and the detailed method of the analysis have been described in Refs. [8,9] and are summarized briefly below. A beam of 240 MeV α particles from the Texas A&M K500 superconducting cyclotron, after passing through a beam analysis system, bombarded self-supporting ^{46,48}Ti foils 2.06 mg/cm^2 and 5.75 mg/cm^2 thick, enriched 83.8% and 99.36% respectively, located in the scattering chamber of the multipole-dipole-multipole (MDM) spectrometer [10]. Scattered particles entering the MDM spectrometer were momentum-analyzed and measured by a focal plane detector which consisted of four resistive wire proportional counters, an ionization chamber, a plastic scintillator and a vertical drift chamber. The proportional counters measured position in the momentum analysis plane, the ionization chamber measured energy losses of the particles, and the scintillator behind the ionization chamber measured the total energy and generated fast timing signals. The in-plane angle was obtained from the positions measured with the four proportional counters and a comparison with RAYTRACE [11] predictions. The vertical drift chamber measured position and angle perpendicular to the momentum analysis plane. The in-plane position and scattering angle resolution were approximately 0.9 mm and 0.09°. The out-of-plane scattering angle was not measured for ^{46}Ti but was measured for ^{48}Ti with a resolution of 0.20°.

The spectrometer angle θ_{spec} and the slit openings defining the solid angles used for the measurements are shown in Table I. The data for each run were binned into ten angle bins by the horizontal angle. The scattering angle for each angle bin was obtained by integrating over the vertical opening of the slit. The differential cross section was extracted from the number of beam particles collected, the target thickness, the solid angle, the yields measured and the dead time. The number of beam particles was monitored with a monitor detector at a fixed scattering angle in the scattering chamber. Dead time of the data taking system was measured by comparing the number of pulses sent to the system to those accepted. The cumulative uncertainties result in about a ±10% uncertainty in absolute cross sections.

Figure 1 shows the angular distribution of the differential cross sections for elastic scattering and inelastic scattering to the first 2^+ state for both nuclei. Experimental data are shown by the circles and the error bars include uncertainty from statistical as well as systematic error. As the ^{46}Ti target was enriched about 84%, angular distributions for both elastic and inelastic scattering in ^{46}Ti include contribution from other Ti isotopes, predominantly ^{48}Ti. Fits were carried out to the angular distributions of the elastic scattering cross sections in order to obtain potential parameters for a density dependent single folding potential with a Woods-Saxon imaginary term [12] and are shown in Fig. 1. Potential parameters obtained for ^{46}Ti were used as initial values in the fit to the elastic scattering data for ^{48}Ti. Table II shows the potential parameters obtained and the parameters of the two-parameter Fermi density distribution of the ground state for both nuclei [13]. Calculations with these potential parameter sets using electromagnetic $B(E2)$ values [14] and collective model transition potentials successfully reproduced the angular distributions of

*Present address: Nuclear Physics Division, Bhabha Atomic Research Center, Mumbai 400085, India.

TABLE I. The spectrometer angles (θ_{spec}) used for measuring the elastic and inelastic scattering for ^{46,48}Ti. The number in parenthesis is the slit opening used (horizontal × vertical in degrees).

	^{46}Ti		^{48}Ti	
	Elastic	GR	Elastic	GR
θ_{spec}	4°∼26° (4 × 2) 29°, 32°, 35° (4 × 4)	0°, 3.5° (4 × 4)	4°, 6°, 8° (4 × 4)	0° (5 × 5) 4°, 6° (4 × 4)

the differential cross sections for the first excited states for each target as can be seen in Fig. 1.

Examples of inelastic scattering spectra for ^{46,48}Ti are shown in Fig. 2. Inelastically scattered α particles corresponding to an excitation energy range of ∼9 to 55 MeV were measured over the full solid angle of the spectrometer. A continuum of events consisting of various reactions such as multistep excitation, pickup-breakup, and knock-out reactions as well as possible background from slit scattering is present above the particle decay threshold. This "continuum" was assumed to start around particle threshold energies [15] ($E_x = 8$ MeV and 9.4 MeV in ^{46,48}Ti, respectively) and increase smoothly. A "continuum curve" with a Fermi shape to model particle threshold effects joining a line roughly following the data above 40 MeV excitation separated the events into a peak and a continuum. The solid lines in Fig. 2 show the range of continuum curves assumed for the analysis.

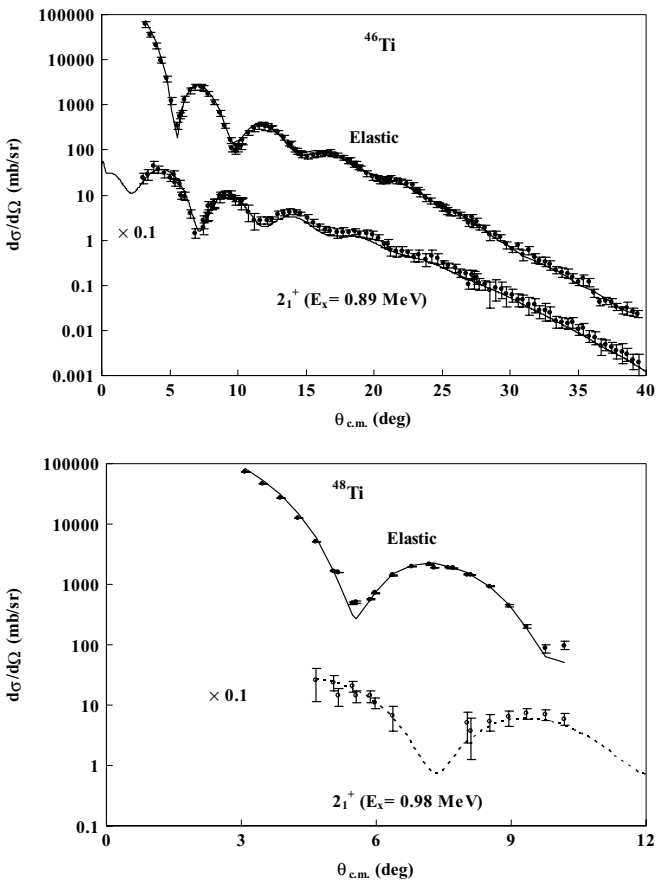

FIG. 1. The angular distributions of the differential cross sections for α particle elastic scattering and scattering to the first excited states for ^{46}Ti and ^{48}Ti. The inelastic scattering cross sections are shown multiplied by 0.1. The lines in both plots are the fits for the elastic scattering and calculated inelastic scattering cross sections using the reduced electric quadrupole transition probability $B(E2)$ for the first excited states.

The giant resonance (GR) peak and the continuum were divided into energy bins spaced evenly in excitation energy. Angular distributions of the giant resonance peak and the continuum for each energy bin were fitted with distorted wave Born approximation (DWBA) calculations for isoscalar $L = 0 - 4$ excitations. The transition density for $L = 0$ was taken as the breathing mode [16] and for $L \geqslant 2$ the Bohr-Mottelson model [16] was used. The transition density for the isoscalar giant dipole resonance (ISGDR) was given by Harakeh and Dieperink [17], which was described for only one of magnetic substates and must be multiplied by $(2l + 1)^{1/2}$ to represent excitation of the ISGDR by α particles. The isovector giant dipole resonance (IVGDR) contributions were small, but were calculated from the known distributions [18,19] and held fixed in the fits. The deformation lengths $(\beta R)_U$ of transition potentials for each multipole were assumed to be equal to nuclear matter deformation lengths $(\beta c)_m$. The calculations were carried out with the code PTOLEMY [20]. Input parameters for PTOLEMY were modified [21] to obtain a relativistic kinematically correct calculation. Figures 3 and 4 show samples of angular distributions for the GR peak and the continuum in ^{46,48}Ti, respectively. Also shown are the multipole fits.

TABLE II. Folding model parameters obtained from fits to elastic scattering and the density parameters (Fermi type) for the ground state.

	V (MeV)	V_I (MeV)	R_I (fm)	A_I (fm)	c (fm)	a (fm)
^{46}Ti	42.826	32.160	4.647	0.938	3.8401	0.550
^{48}Ti	33.699	32.913	4.896	0.862	3.8185	0.550

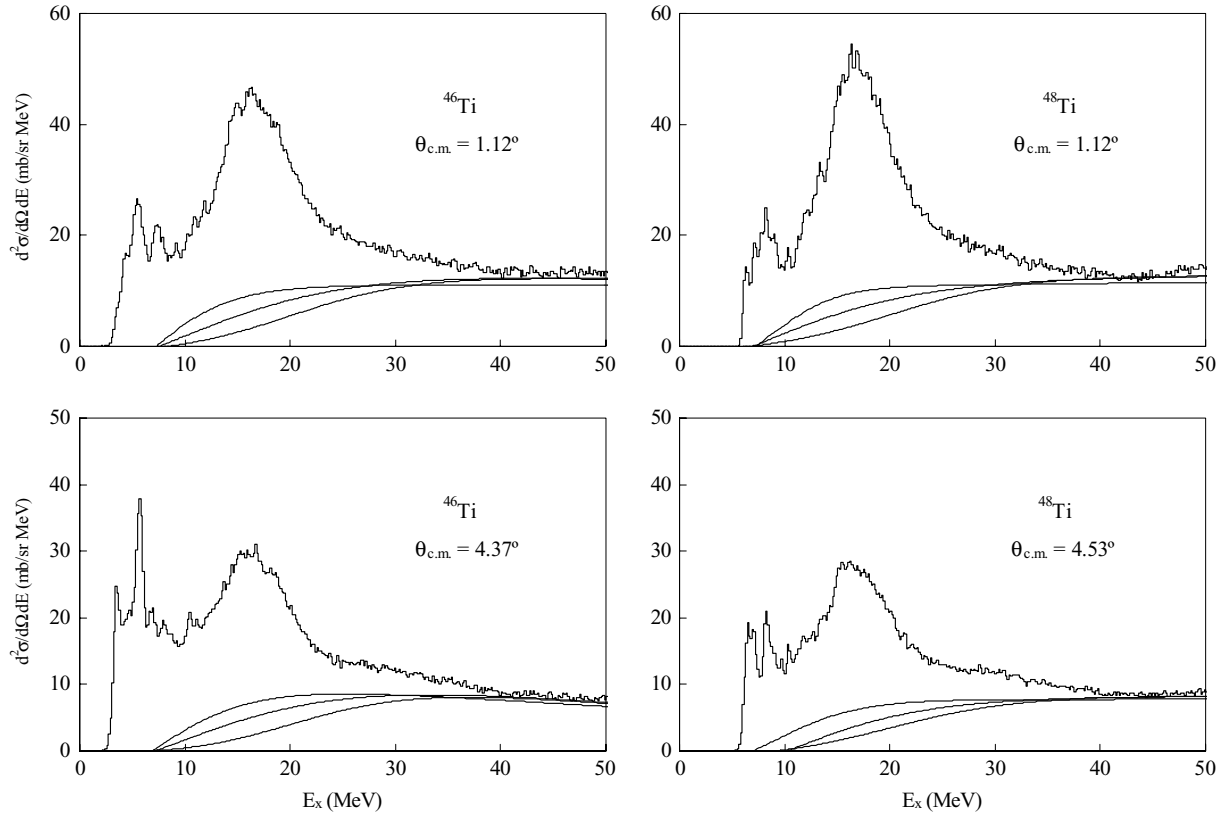

FIG. 2. Excitation energy spectra for ^{46,48}Ti. Experimental data are shown by the histograms. The solid lines in the figures show the range of continuum curves chosen for the analysis.

III. RESULTS AND DISCUSSION

EWSR strength distributions were obtained with several choices of the continuum curves. To determine the influence of the choice of continuum on the distributions, the amplitude, slope, and thresholds of the continuum curves were changed. Weighted averages of the strength distributions obtained are shown in Fig. 5. The error bars consist of the errors obtained from the fit and the errors due to the choice of the continuum curve determined from the standard deviation of the different strength distributions [22]. The uncertainty was determined for each multipole in the multipole fit by incrementing (or decrementing) that strength, then adjusting the strength of the other multipoles to minimize total χ^2. This continued until the new χ^2 was one unit larger than the total χ^2 obtained for the best fit. The errors on the strength distributions were obtained by adding the standard deviations between the results obtained from the different continua choices to the errors obtained from the multipole fits in quadrature.

GR peak cross sections obtained after subtracting continuum curves had poor statistics above 32 MeV in excitation energy. The angular range measured for ^{46}Ti was limited, so that the $L = 3$ component was not separated from higher multipoles. The experimental data were not analyzed above $E_x = 39$ MeV because α particles from the pickup-breakup reaction ($^5\mathrm{Li} \rightarrow \alpha + p$) would be in the spectrum above 39 MeV in both ^{46}Ti and ^{48}Ti. Parameters obtained for the strength distributions for each target are listed in Table III.

Angular distributions of the continuum were also fitted with the DWBA calculations to see if there were obvious peaking in the multipole strength functions obtained from the continuum that might be attributed to multipole resonances. About 10% or less of $E0$ EWSR was obtained in a small bump around 18 MeV which died off above 26 MeV. This is included in the $E0$ strength distributions shown in Fig. 5. The strength distributions for other multipoles extracted from the continuum distributions increased monotonically at higher excitation and are likely dominated by contributions from different reaction mechanisms.

A total of 71 + 15/−12% and 96 + 14/−12% of the $E0$ EWSR, including both the peak and the continuum contributions, were found with a centroid (m_1/m_0) of 18.66 + 0.65/−0.25 MeV and 18.80 + 0.45/−0.18 MeV in ^{46}Ti and ^{48}Ti, respectively. $E0$ strength in both nuclei is concentrated in a Gaussian-like peak that tailed to higher excitation. Such tailing was not observed for heavier targets [22,23], but has been observed and predicted in ^{58}Ni [6,24] and ^{90}Zr [25,26] and might be an indication of a fragmentation of the strength.

TABLE III. Parameters obtained for isoscalar multipole giant resonances in ^{46,48}Ti.

^{46}Ti	Moments							
	$E0$	Error	$E1$	Error	$E2$	Error	$E3$ + higher	Error
m_1	0.71	+0.15	0.46	±0.12	0.60	±0.11	0.73	±0.11
(Frac EWSR)		−0.12						
m_1/m_0	18.66	+0.65	22.77	+0.43	16.38	+0.17	21.38	±0.14
(MeV)		−0.25		−0.40		−0.14		
rms width	5.12	+1.24	7.91	±0.20	3.47	+0.51	7.93	±0.18
(MeV)		−0.36				−0.44		
$(m_3/m_1)^{1/2}$	20.47	+1.41	26.44	+0.65	17.39	+0.50	25.18	±0.25
(MeV)		−0.49		−0.62		−0.43		
$(m_1/m_{-1})^{1/2}$	18.10	+0.50	21.36	+0.31	16.05	+0.12	19.98	±0.12
(MeV)		−0.20		−0.28		−0.10		
^{48}Ti	Moments							
	$E0$	Error	$E1$	Error	$E2$	Error	$E3$	Error
m_1	0.96	+0.14	0.56	±0.12	0.87	±0.11	0.43	±0.11
(Frac EWSR)		−0.12						
m_1/m_0	18.80	+0.45	23.85	+0.40	16.94	+0.17	24.84	±0.27
(MeV)		−0.18		−0.36		−0.14		
rms width	4.51	+1.27	7.02	+0.21	3.72	+0.60	7.25	±0.20
(MeV)		−0.20		−0.17		−0.46		
$(m_3/m_1)^{1/2}$	20.25	+0.99	26.76	+0.57	18.07	+0.44	28.12	±0.39
(MeV)		−0.28		−0.50		−0.35		
$(m_1/m_{-1})^{1/2}$	18.33	+0.36	22.69	+0.32	16.55	+0.12	23.18	±0.20
(MeV)		−0.15		−0.29		−0.10		

The $E2$ strength in ^{46,48}Ti was centered at 16.38 + 0.17/−0.14 MeV and 16.94 + 0.17/−0.14 MeV and exhausted 60±11% and 87±11% of the $E2$ EWSR, respectively. The shape is almost Gaussian. The $E2$ strength is somewhat sensitive to continuum choices and changes about ±7% when the continuum curves were chosen within the range shown in Fig. 2, however, this had little effect on the peak energies.

The $E3$ strength in nuclei is split into two modes, the low-energy octupole resonance (LEOR) and the high-energy octupole resonance (HEOR). Approximately 75% of the $E3$ EWSR should be in the HEOR [27]. A total of 43±11% of the $E3$ EWSR in ^{48}Ti was located with a centroid 24.84±0.27 MeV and consists of two components. The high excitation component (39±11%) is centered at 27.89±0.33 MeV. The "missing" strength may be subtracted out as part of the continuum or some could be above E_x = 39 MeV. The $E3$ strength in ^{46}Ti could not be separated from higher multipoles due to the limited angular range, but if all of the observed strength is assumed to be $L = 3$, then it would correspond to 73±11% of the $L = 3$ EWSR. The centroid of the strength is 21.38±0.14 MeV.

A total of 46±12% and 56±12% of the isoscalar $E1$ EWSR in ^{46,48}Ti was located with centroids of 22.77 + 0.43/−0.40 MeV and 23.85 + 0.40/−0.36 MeV, respectively. The strength distribution was spread from 10 MeV through around 38 MeV. The $E1$ strength consists of two components which have been observed from light to heavy nuclei [5,8,22,23,28]. The high-energy component is the compression mode [29], while it has been suggested that the low-energy component might be a "toroidal giant dipole mode" [30,31]. The $E1$ distributions were fit with two Gaussians and parameters obtained are shown in Table IV. The low-energy components in ^{46,48}Ti have 10±4% and 13±5% of the $E1$ EWSR, respectively, with centroids of 15.9±0.3 MeV and 16.8±0.3 MeV, respectively. The high-energy components contain 34±10% and 43±9% of $E1$ EWSR with centroids of 28.3±0.7 MeV and 28.8 + 0.8/−0.7 MeV in ^{46,48}Ti, respectively.

The energies of the high-energy components of the $E1$ strength in both nuclei are much lower than expected from scaling model calculations ($(m_3/m_1)^{1/2} \sim 35$ MeV) [4]. Since considerably less than 100% of $E1$ EWSR was located in ^{46}Ti and ^{48}Ti, it is likely that some of the $E1$ strength is located above the E_x = 39 MeV.

Figure 6 shows the mass dependence of E_{GMR} in ^{46,48}Ti, ^{40}Ca and ^{58}Ni together with theoretical calculations obtained in the scaling model using the leptodermous expansion of the finite-nucleus incompressibility K_A. Non-relativistic calculations using the extended Thomas-Fermi (ETF) approximation with the SkM* Skyrme interaction ($K_{\mathrm{NM}} = 216.6$ MeV) by Nayak *et al.* [7] and relativistic calculations using the relativistic mean-field (RMF) theory with the NLC interaction

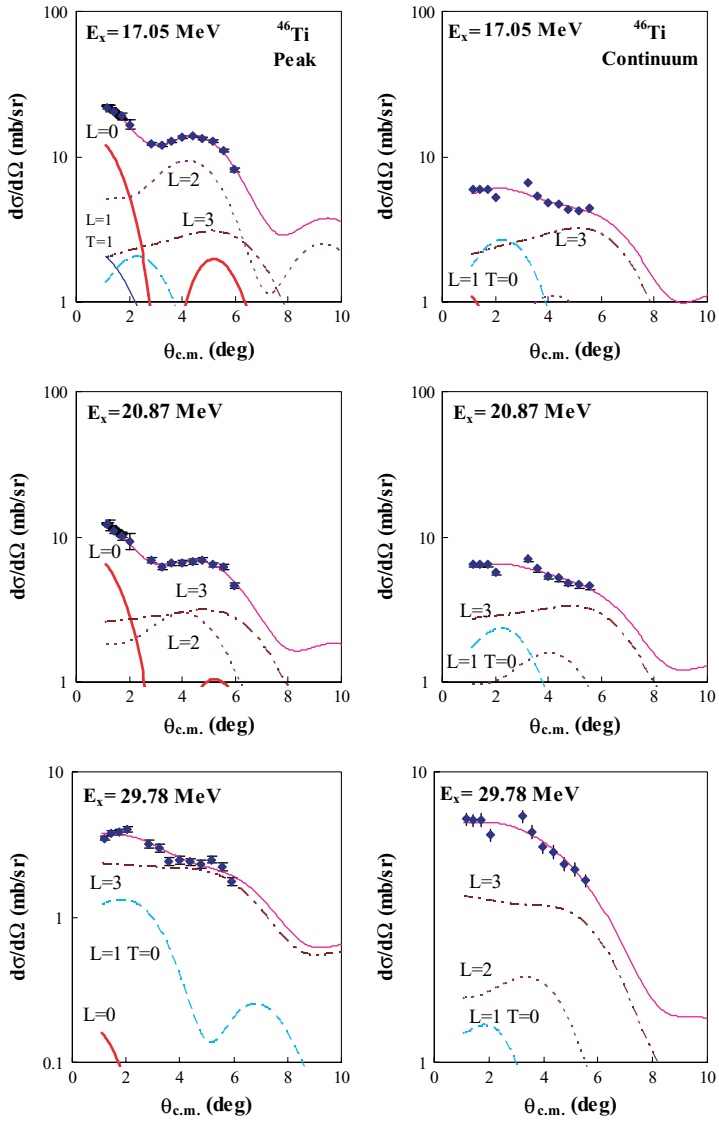

FIG. 3. (Color online) Angular distributions of the cross sections for the GR peak and the continuum in ^{46}Ti. The excitation energies are the center energies of excitation energy bins which are 0.64 MeV wide. Experimental data are shown by solid squares. Each experimental point has an error bar from the statistics and standard deviation where more than one data point was available. The results of the multipole fits are shown along with each multipole, $L = 0$, 1, 2, 3, and IVGDR components shown by the thick solid, dashed, dot, dashed-dot, and solid lines, respectively.

TABLE IV. Parameters obtained with Gaussian fits for isoscalar multipole giant resonances in ^{46,48}Ti.

^{46}Ti	Gaussian fits							
	$E0$	Error	$E1$ Peak 1	Error	$E1$ Peak 2	Error	$E2$	Error
Centroid (MeV)	18.44	±0.25	15.94	±0.31	28.30	±0.68	16.79	±0.19
FWHM (MeV)	9.23	±0.10	6.34	$+0.63$ -0.50	14.35	$+0.65$ -0.79	7.66	±0.11
Fraction EWSR	0.62	±0.11	0.10	±0.04	0.34	±0.10	0.59	±0.11
^{48}Ti	Gaussian fits							
	$E0$	Error	$E1$ Peak 1	Error	$E1$ Peak 2	Error	$E2$	Error
Centroid (MeV)	18.73	±0.23	16.75	$+0.31$ -0.28	28.82	$+0.78$ -0.72	17.47	±0.20
FWHM (MeV)	8.28	±0.05	7.27	$+0.22$ -0.24	12.44	$+0.56$ -0.68	7.62	±0.12
Fraction EWSR	0.84	±0.11	0.13	±0.05	0.43	±0.09	0.83	±0.11

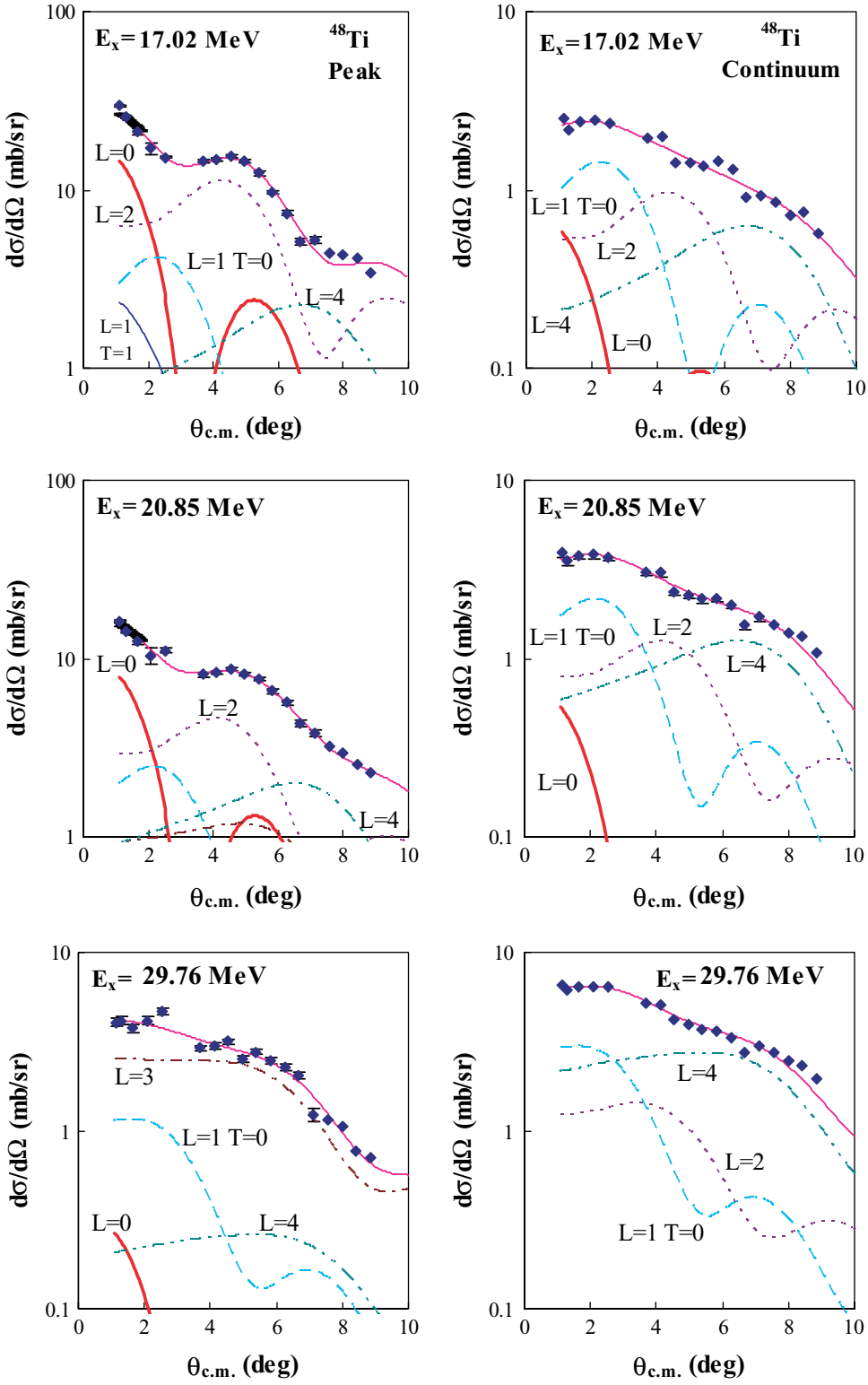

FIG. 4. (Color online) Angular distributions of the cross sections for the GR peak and the continuum in ^{48}Ti. The excitation energies are the center energies of excitation energy bins which are 0.64 MeV wide. Experimental data are shown by solid squares. Each experimental point has an error bar from the statistics and standard deviation where more than one data point was available. The results of the multipole fits are shown along with each multipole, $L = 0$, 1, 2, 3, 4 and IVGDR components shown by the thick solid, dashed, dot, dashed-dot, dashed-double-dot, and solid lines, respectively.

($K_{\rm NM}$ = 224.5 MeV) by Chossy and Stocker [32] are also shown in Fig. 6. The GMR energies for ^{40}Ca, ^{46}Ti, and ^{48}Ti are in good agreement with the non-relativistic theoretical calculation whereas that for ^{58}Ni is well above the calculation. The predictions using the RMF calculations with the NLC interaction are in agreement with the ^{58}Ni energy [6] but are higher than the data for ^{40}Ca, ^{46}Ti, and ^{48}Ti. The $E_{\rm GMR}$ was obtained from the theoretical finite nucleus incompressibility K_A using the rms charge radius, which is available from experiments, rather than the rms matter radius.

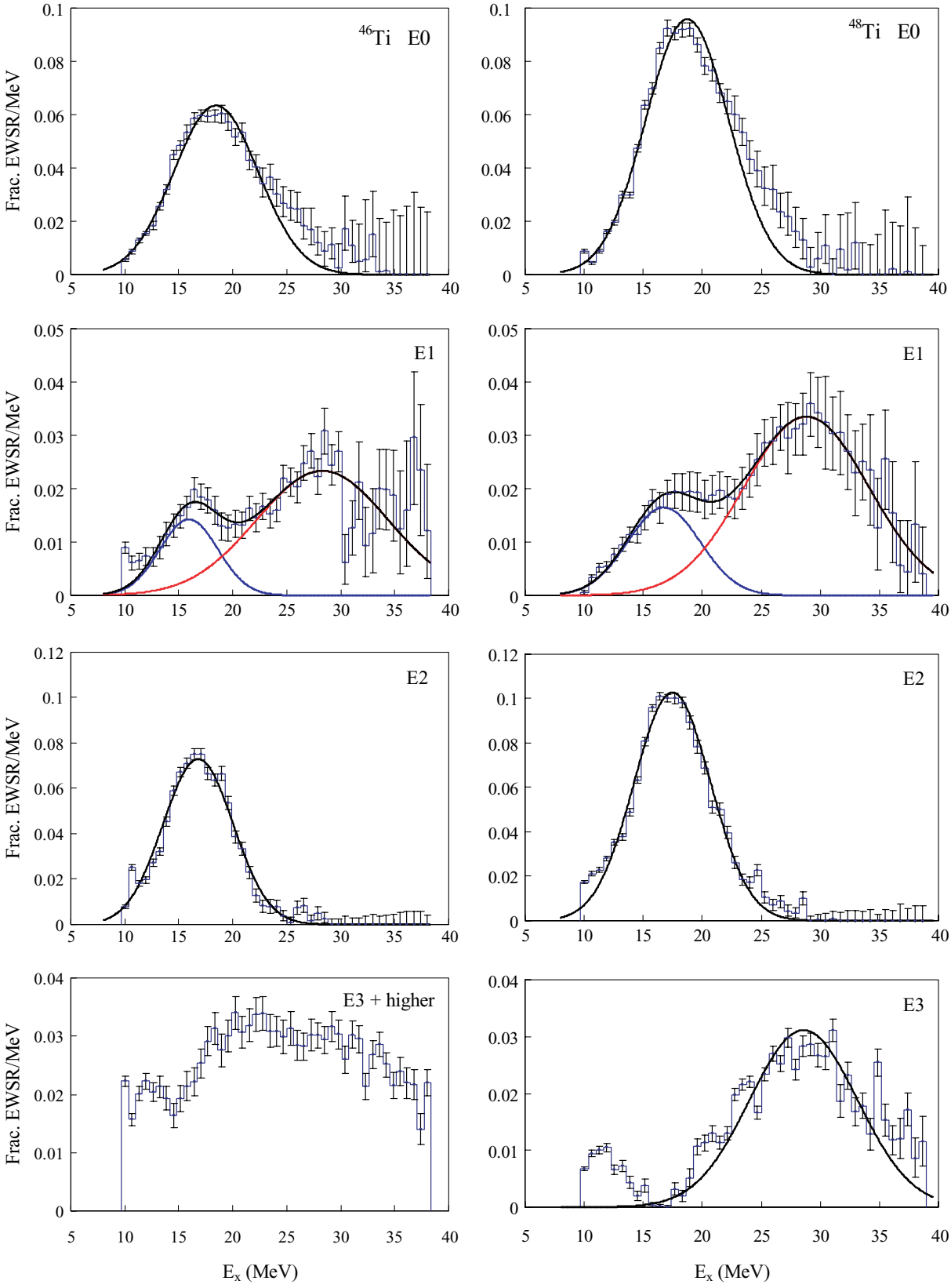

FIG. 5. (Color online) Strength distributions obtained for ^{46,48}Ti are shown by the histograms. Error bars represent the uncertainty due to the fitting of the angular distributions and different choices of the continuum as described in the text. The smooth lines show Gaussian fits.

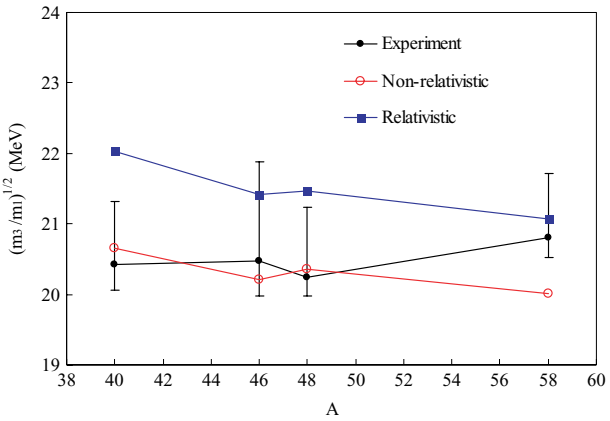

FIG. 6. (Color online) GMR energies ($E_{GMR} = (m_3/m_1)^{1/2}$) as a function of mass number for nuclei with $A = 40$–58. The solid circles represent the experimental data. The open circles show results obtained using the extended Thomas-Fermi (ETF) approximation with a Skyrme interaction (SkM*) [7] and solid squares show results obtained using the relativistic mean-field (RMF) theory with the NLC interaction [32]. The lines are added to guide the eye.

IV. CONCLUSIONS

The GMR in ^{46,48}Ti was investigated using inelastically scattered 240 MeV α particles. A total of 71 + 15/−12% and 96 + 14/−12% of the $E0$ EWSR was observed in ^{46}Ti and ^{48}Ti, respectively, with a tail on the higher excitation energy side. Such an asymmetric shape was also observed in nuclei around mass 60 [6] and in ^{90}Zr. $E2$ strength in ^{46}Ti and ^{48}Ti was identified in a Gaussian peak containing 60±11% and 87±11% of EWSR, respectively. The isoscalar $E1$ strength in ^{46,48}Ti consists of two components as in heavier nuclei. A total of 46±12% and 56±12% of the $E1$ EWSR in ^{46}Ti and ^{48}Ti was found, respectively, and these are consistent with that found in ^{40}Ca (21 + 3/−7%)[1] and ^{58}Ni (68 + 20/−15% [6]). About 40% of HEOR in ^{48}Ti was identified with a centroid of around 28 MeV and about 70% of $L \geqslant 3$ strength in ^{46}Ti was identified with a centroid of around 25 MeV. The GMR energies in the Ti isotopes are described well using the leptodermous expansion to interpolate energies calculated for other nuclei with the SkM* interaction ($K_{NM} =$ 216.6 MeV) which also reproduces the ^{40}Ca GMR energy. However the GMR energy in ^{58}Ni is substantially higher than predicted.

ACKNOWLEDGMENTS

This work was supported in part by the U.S. Department of Energy under Grant No. DE-FG02-93ER40773 and by the Robert A. Welch Foundation.

[1] It was reported that the total $E1$ EWSR in ^{40} Ca was 62+ 10/−20% [15]. However this was obtained taking only one magnetic substate into account in the transition potential [17].

[1] A. van der Woude, Prog. Part. Nucl. Phys. **18**, 217 (1987).
[2] A. van der Woude, Nucl. Phys. **A649**, 97c (1999).
[3] J. P. Blaizot, Phys. Rep. **64**, 171 (1980).
[4] S. Stringari, Phys. Lett. **B108**, 232 (1982).
[5] D. H. Youngblood, Y.-W. Lui, H. L. Clark, Y. Tokimoto, and B. John, Phys. Rev. C **68**, 057303 (2003).
[6] Y.-W. Lui, D. H. Youngblood, H. L. Clark, Y. Tokimoto, and B. John, Phys. Rev. C **73**, 014314 (2006).
[7] R. C. Nayak, J. M. Pearson, M. Farine, P. Gleissl, and M. Brack, Nucl. Phys. **A516**, 62 (1990).
[8] D. H. Youngblood, Y.-W. Lui, and H. L. Clark, Phys. Rev. C **60**, 014304 (1999).
[9] D. H. Youngblood, Y.-W. Lui, and H. L. Clark, Phys. Rev. C **65**, 034302 (2002).
[10] D. M. Pringle, W. N. Catford, J. S. Winfield, D. G. Lewis, N. A. Jelley, K. W. Allen, and J. H. Coupland, Nucl. Instrum. Methods Phys. Res. A **245**, 230 (1986).
[11] S. Kowalski and H. A. Enge (unpublished).
[12] G. R. Satchler and D. T. Khoa, Phys. Rev. C **55**, 285 (1997).
[13] H. D. Wohlfahrt, E. B. Shera, and M. V. Hoehn, Y. Yamazaki, and R. M. Steffen, Phys. Rev. C **23**, 533 (1981).
[14] S. Raman, C. W. Nestor Jr., and P. Tikkanen, At. Data Nucl. Data Tables **78**, 1 (2001).
[15] D. H. Youngblood, Y.-W. Lui, and H. L. Clark, Phys. Rev. C **63**, 067301 (2001).
[16] G. R. Satchler, Nucl. Phys. **A472**, 215 (1987).
[17] M. N. Harakeh and A. E. L. Dieperink, Phys. Rev. C **23**, 2329 (1981).
[18] R. E. Pywell and M. N. Thompson, Nucl. Phys. **A318**, 461 (1979).
[19] R. Sutton, M. N. Thompson, M. Sugawara, K. Shoda, T. Saito, and H. Tsubota, Nucl. Phys. **A339**, 125 (1980).
[20] M. Rhoades-Brown, M. H. Macfarlane, and S. C. Pieper, Phys. Rev. C **21**, 2417 (1980); **21**, 2436 (1980); M. H. Macfarlane and S. C. Pieper, Argonne National Laboratory Report No. ANL-76-11, Rev. 1, 1978 (unpublished).
[21] G. R. Satchler, Nucl. Phys. **A540**, 533 (1992).
[22] D. H. Youngblood, Y.-W. Lui, H. L. Clark, B. John, Y. Tokimoto, and X. Chen, Phys. Rev. C **69**, 034315 (2004).
[23] Y.-W. Lui, D. H. Youngblood, Y. Tokimoto, H. L. Clark, and B. John, Phys. Rev. C **69**, 034611 (2004).
[24] S. Kamerdzhiev, J. Speth, and G. Tertychny, Eur. Phys. J. A **7**, 483 (2000).
[25] D. H. Youngblood, Y.-W. Lui, B. John, Y. Tokimoto, H. L. Clark, and X. Chen, Phys. Rev. C **69**, 054312 (2004).
[26] I. Hamamoto, H. Sagawa, and X. Z. Zhang, Phys. Rev. C **56**, 3121 (1997).
[27] J. M. Moss, D. H. Youngblood, C. M. Rozsa, D. R. Brown, and J. D. Bronson, Phys. Rev. Lett. **37**, 816 (1976); H. P. Morsch, M. Rogge, P. Turek, and C. Mayer-Boricke, *ibid.* **45**, 337 (1980); T. Yamagata, S. Kishimoto, K. Yuasa, K. Iwamoto, B. Saeki, M. Tanaka, T. Fukuda, I. Miura, M. Inoue, and H. Ogata, Phys. Rev. C **23**, 937 (1981); P. F. Bortignon and R. A. Broglia, Phys. Lett. **B102**, 303 (1981).

[28] H. L. Clark, Y.-W. Lui, and D. H. Youngblood, Phys. Rev. C **63**, 031301(R) (2001).
[29] G. Colo, N. Van Giai, P. F. Bortignon, and M. R. Quaglia, Phys. Lett. **B485**, 362 (2000).
[30] D. Vretenar, N. Paar, P. Ring, and T. Niksic, Phys. Rev. C **65**, 021301(R) (2002).
[31] G. Colo and Nguyen Van Giai, Nucl. Phys. **A731**, 15 (2004).
[32] T. v. Chossy and W. Stocker, Phys. Rev. C **56**, 2518 (1997).